Article citation info:
Abbas EN, Abud Ali ZAA, Njim EK, Flayyih MA, Flayyih M, Madan R. Analytical and numerical investigation of free vibration of nanoparticle-reinforced composite cylindrical shells. Diagnostyka. 2025;26(1):2025112. https://doi.org/10.29354/diag/201249.

DIAGNOSTYKA, 2025, Vol. 26, No. 1

e-ISSN 2449-5220
DOI: 10.29354/diag/201249

ANALYTICAL AND NUMERICAL INVESTIGATION OF FREE VIBRATION OF NANOPARTICLE-REINFORCED COMPOSITE CYLINDRICAL SHELLS

Ehab N. ABBAS [1], **Zaman Abud Almalik ABUD ALI** [2], **Emad Kadum NJIM** [3,*], **Mujtaba A. FLAYYIH** [4], **Royal MADAN** [5]

[1] Ministry of Higher Education and Scientific Research, Studies & Planning & Follow-Up Directorate, Baghdad, Iraq
[2] Department of Mechanical Engineering, Faculty of Engineering, University of Kufa, Iraq
[3] Ministry of Industry and Minerals, State Company for Rubber and Tires Industries, Iraq
[4] Prosthetics and Orthotics Engineering Department, College of Engineering and Technologies, Al-Mustaqbal University, Hillah, 51001, Iraq
[5] Department of Mechanical Engineering, Graphic Era, Dehradun 248002, Uttarakhand, India
*Corresponding author, e-mail: emad-njim@scrit.gov.iq

Abstract

This study focuses on the characterization of free vibration of composite shell structures strengthened by different volume fractions of nanoparticles analytically and numerically. Using simply supported boundary conditions, the governing differential equation of motion for the shell was formulated based on the Donnell-Mushtari-Vlasov (DMV) shell theory. For different design parameters, the natural frequency was investigated by employing the Orthogonality method. Four different layers of material, namely Perlon, Carbon, Kevlar, and Kenaf, of thickness 30 mm, were made. Nanoparticles Alumina (Al_2O_3) and Silica (SiO_2) were chosen and mixed in varying volume fractions (0.5%, 1%, 1.5%, 2%, and 2.5%) for the sample fabrication. Two types of samples, A and B, were created based on the arrangement of layers. The tensile tests were performed on the fabricated specimens to identify the longitudinal Young's modulus of specimens. The two groups that consist of different layers of materials were made and named as group A and group B. The results indicate an increase in Young's modulus of 33.9% increase for nano Al_2O_3 and a 42.25% increase for nano SiO_2 at a volume fraction of 2.5% for group A, while for group B, the enhancement was 37.96% and 47.39% for Al_2O_3 and SiO_2 nanoparticles, respectively. The results indicate that as the volume fraction of nanomaterial is increased, the natural frequency increases. The experimental results are used to validate both analytical and numerical solution conducted by the finite element method (FEM) under various loading conditions. The maximum difference between the analytical and numerical prediction of the natural frequency results was within 5%.

Keywords: cylindrical shell structure, free vibration frequency, nanoparticles, FEM

NOMENCLATURE

R	The radius of the cylinder (mm)
L	The length of the shell (mm)
V_f	Volume fraction %
E	Modulus of elasticity (GPa)
ν	Poisson's ratio
ρ	The mass density of shell material (kg/m^3)
ω	Natural frequency (rad/sec)
ψ	Non-dimensional parameter of the natural frequency

1. INTRODUCTION

Compared with classical designs, nanocomposite structures exhibit unusual property combinations and can be designed in various ways with high-performance materials [1-3]. Curved surfaces characterize structural membranes or shells and can distribute loads in multiple directions. Properly constructed, shaped, proportioned, and supported, they maintain structural integrity without bending or twisting. Thin shells specifically refer to shells with relatively small thicknesses. However, they should not be excessively thin to the point of causing significant deformations and are widely used in various aerospace, architectural, civil, marine, and mechanical engineering areas as load-carrying segments [4-6]. The existence of shell structures in these applications induced researchers to understand their behavior to increase efficiency and avoid failure [7]. Therefore, several theories have been published so far on different types of material. Also,

Received 2024-06-07; Accepted 2025-02-11; Available online 2025-02-12

various methods, including analytical, experimental, and numerical techniques, were studied to examine the dynamic response of composite structures [8-10].

Based on first-order shear deformation theory, Javed et al. [11] investigated the dynamics of non-uniform cylindrical shells. An E-glass/epoxy (EGE) composite laminate shell was constructed from Kevlar-49/epoxy composite materials arranged in different orders. Several anti-symmetric angle ply layers were arranged in layers under different boundary conditions to achieve a shell with a non-uniform thickness. Helloty et al. [12] examined the impact of laminated shell composite materials and boundary conditions on the dynamic response of structures under different loads using the finite element method. Chaubey et al. [13] developed a formulation of finite elements that incorporates the third-order shear deformation theory (TSDT) to calculate the non-dimensional natural frequency of composite shells. This formulation also takes into account the presence of concentrated mass and cutouts in the shell structure. The suggested model provides zero transverse shear stress conditions at the shell structure in the head and base without employing a shear correction factor.

Under extreme boundary conditions, Li et al. [14] proposed a new semi-analytical method for solving the influence of free vibration problem on functionally graded porous (FGP) shell composite by utilizing the energy method and first-order shear deformation theory (FSDT). Two typical types of porosity distributions employed in the study were symmetric and nonsymmetrical models. Wang et al. [15] performed free vibration behavior on a metal foam composite cylindrical shell. They specifically focused on the assumed governing variables that dictate the system characteristics i.e., the natural frequency and mode shapes. Dongze He [16] employed a wave-based method to analyze the free vibration of composite laminated cylindrical shells. The study considered shells with both restrained elastic boundaries and general classical boundaries. The analysis aimed to understand the vibration behavior of these shells under various conditions. Ghasemi et al. [17] utilized the modified couple stress theory (MCST) to investigate the frequencies of micro and nano-fiber-metal laminate (FML) cylindrical shells. This study focused on analyzing the vibration characteristics and behavior of FML cylindrical shells using the MCST approach.

Using the finite element method (FEM), Tran et al. [18] investigated laminated graphene nanoplatelets reinforced composite shells. In this paper, using first-order shear deformation theory, an 8-node iso-parametric element has been used to determine the oscillation equation for shell structure. According to Zhang et al. [19], sandwich shells resting on the Pasternak foundation exhibit various vibrational behaviors under humid conditions. A composite laminated spherical shell was examined using Fourier series discretization techniques [20]. Experimental, analytical, and ABAQUS/CAE analyses were conducted by M Q. Wu et al. [21] to examine the nonlinear dynamic response of two-dimensional square shallow composite laminated shells reinforced by carbon fiber under foundation excitation.

Several laminated composite shells and spatial structures were examined by conducting free vibration analysis by Chen et al. [22]. Utilized the moving-least-squares approximation to develop a mesh-free FSDT method. FG carbon nanotube-reinforced composite panels with sinusoidal corrugation were studied using iso-geometric analysis by Muhammadi et al. [23]. Ameer Melaibari et al. [24] applied a novel analytical technique based on Galerkin's theory in the study of composite laminated shells reinforced with single-walled carbon nanotubes at random orientations. Five types of shell shapes with different geometrical properties are considered in this study. Kuo Tian et al. [25] used a numerical vibration correlation method and optimization design to improve the buckling load of composite cylindrical shells loaded axially. Lin et al. [26] investigated the dynamic stability of cylindrical fiber composite shells with metal liners under uniform pressure pulses by combining finite element simulations and theoretical modeling. Using a semi-analytical approach, Haichao Li [27] studied the free vibrations of laminated composite cylindrical and spherical shells subjected to complex boundary conditions using multi-segment partitioning strategies. According to Sandipan Nath Thakur [28], moderately thick hyperbolic paraboloidal laminated shells exhibit effective response behavior in the presence of higher-order shear deformation theory (HSDT). Donnell's shell theory has been combined with the refined Halpin-Tsai micromechanical approach in a study conducted by Zamani [29]. Laminated composite conical shells reinforced by graphene sheets were investigated for their free vibration behaviors. Using the finite element method (FEM), K. Kim et al. [30] studied elliptical-cylindrical-elliptical laminated composite shells with elastic boundary conditions. A stepped and stiffened cylindrical shell structure subjected to arbitrary boundary conditions was analyzed using stepped and stiffened shear deformation theory and the finite element method [31]. A study by Logesh, et al. [32] evaluated the effect of nanoparticles (Al_2O_3-SiO_2) on the mechanical properties of blended matrix polymer composites.

Free vibration of porous graphene nano-platelet (GNP) nano-enrichment composite spheroidal-cylindrical shells was performed by estimating the properties of the composite by using the rule of mixture and Halpin-Tsai homogenization techniques [33]. Free vibration studies on shell structures reinforced with SiO_2 were performed by employing the finite element method and semi-analytical approach [34, 35]. From the host of literature, it was found that the rule of mixture is inadequate in estimating the material properties effectively [36, 37]. Accurate estimation of material properties, such as Young's modulus and density, is critical as they serve as inputs for analytical and finite element analysis. Incorrect estimation of these properties can lead to erroneous predictions such as natural frequency in the present study. Therefore, one of the key objectives of the present work is to experimentally determine the material properties and use these values to predict the natural frequency of Al_2O_3 and SiO_2-reinforced structures using established methods.

Additionally, the shell structure can be used as an orthosis or prosthetic part; thus, it was necessary to incorporate reinforcement into the shell structure to determine its mechanical characteristics. Nanoparticles can be used as reinforcement materials for enhancing the mechanical and dynamic characteristics. Then, the reinforcement of nanoparticle materials changes the stiffness-to-weight ratio. So, the new contribution of this work is to modify the mechanical and dynamic characterizations of shell structure by reinforcing it with nanoparticle materials to achieve high strength and high mechanical and dynamic performance. Various interesting findings are presented here concerning the static and dynamic analysis of nanocomposite laminated thin shell structure. A unified formulation to investigate the vibration behaviors of cylindrical shells subjected to arbitrary boundary restraints was performed. This formulation is based on various parameters such as volume fraction, nanoparticle type, and boundary conditions.

2. MATERIALS AND METHODS

In the literature, numerous researchers employed different experimental techniques focusing on the behavior of nanocomposite structures [38, 39]. In the current study, the experiment program consists of two parts: the first one is preparing samples with and without nanomaterials (Al_2O_3 & SiO_2), and the second part is related to obtaining Young's modulus by performing tensile tests. The samples were produced from the fibers materials (Perlon, Carbon, Kevlar, Kenaf, Resin, Hardener, and two types of nanoparticles) as illustrated in Figure 1. The specimens were created in the form of layering reinforced materials that were pressed for each sample in groups A and B, as shown in Table 1-3. Figure 1 shows photographic images of the material used and the packaging of Orthocryl Resin and powders of nanoparticles, displaying the product name and brand. This allows researchers and industries to easily procure the product and access important details, such as purity, density, moisture content, chemical composition, safety data, and usage guidelines, among other key specifications.

All the produced specimens are reinforced with two types of nanoparticles with varied volume fractions. Figure 2 illustrates how the production of the combined model with bonding nanomaterials influences the mixing of nanoparticles with thickening liquid in orthocryl resin using an ultrasonic homogenizer device. Figure 3 shows how reinforcement is accomplished by mixing resin and layers of fibers using the vacuum technique. Nanoparticles utilized to improve composite materials are SiO_2 and Al_2O_3 with five values of volume fractions (0.5, 1, 1.5, 2, and 2.5) %.

Young's modulus of elasticity of composite materials with different nanomaterials was determined using the Universal Tensile Machine by

Fig. 1. Materials used in preparing the sample

Fig. 2. Vacuum machine

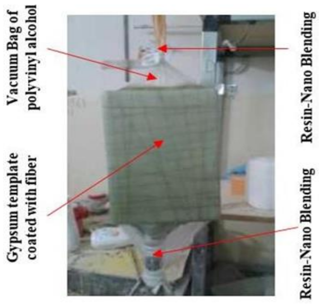

Fig. 3. Materials Manufacturing

following the standard specification (ASTM-D638), as shown in Figure 4. Table 2 shows the ten samples with each volume fraction that were tested for tensile strength.

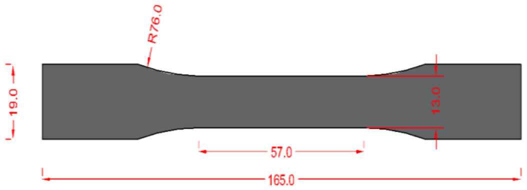

Fig. 4. Geometry of tensile test Specimen According to (ASTM-D638) standard

Table 1. Mechanical properties of composite material used

Group	Number of Layers	E (GPa)	ν	ρ (kg/m^3)
A	1 layer Perlon	16.78	0.22	1180
	2 layer Carbon			
	1 layer Kevlar			
	4 layer Perlon			
	1 layer Kevlar			
	2 layer Carbon			
	1 layer Perlon			
B	1 layer Perlon	17.49	0.18	1210
	2 layer Carbon			
	1 layer Kevlar			
	1 layer Kenaf			
	2 layer Perlon			
	1 layer Kenaf			
	1 layer Kevlar			
	2 layer Carbon			
	1 layer Perlon			

Table 2. Material properties used with different volume fractions of nanomaterials

Group	Nano Al_2O_3 Material			Nano SiO_2 Material		
	S	V_f %	E (GPa)	S	V_f %	E (GPa)
A	A1	0	16.78	A1	0	16.78
	A2	0.5	17.34	A2	0.5	17.92
	A3	1	18.42	A3	1	19.12
	A4	1.5	19.83	A4	1.5	20.33
	A5	2	20.88	A5	2	21.74
	A6	2.5	22.47	A6	2.5	23.87
B	B1	0	17.49	B1	0	17.49
	B2	0.5	18.23	B2	0.5	19.46
	B3	1	19.47	B3	1	20.74
	B4	1.5	20.44	B4	1.5	22.31
	B5	2	21.89	B5	2	23.85
	B6	2.5	24.13	B6	2.5	25.78

Table 3. Details of composite constituents

Item	Group A	Group B
layer Perlon	6	4
layer Carbon	4	4
layer Kevlar	2	2
layer Kenaf	0	2

3. THE ANALYTICAL MODEL

The analytical solutions of the shell structure include constructing an equation of motion for a simply supported shell structure. However, to derive the general vibration shell equation, the following steps are required:

a) Derive the equation of motion for the shell structure considering external load effects.
b) Determine the generalized displacement for the shell by assuming it is a function of the selected coordinates.
c) Calculate the natural frequency using the derived mathematical model.

In this context, the cartesian system coordinates are utilized [34].

$$X = X(\alpha, \beta)$$
$$Y = Y(\alpha, \beta) \qquad (1)$$
$$Z = Z(\alpha, \beta)$$

The two independent coordinates α and β can be used to describe the undeformed middle surface of a thin shell; therefore, the following assumptions for small displacement theory apply as follows:

- Small thickness compared to other shell dimensions.
- Minimal shell strain and displacement.
- Negligible stress in the z-direction.
- The normal to the undeformed middle surface does not undergo any extension or contraction, even after deformation. It maintains its straightness and remains perpendicular to the middle surface throughout the deformation process. Then, the displacement representation of the shell is assumed as [40,41]:

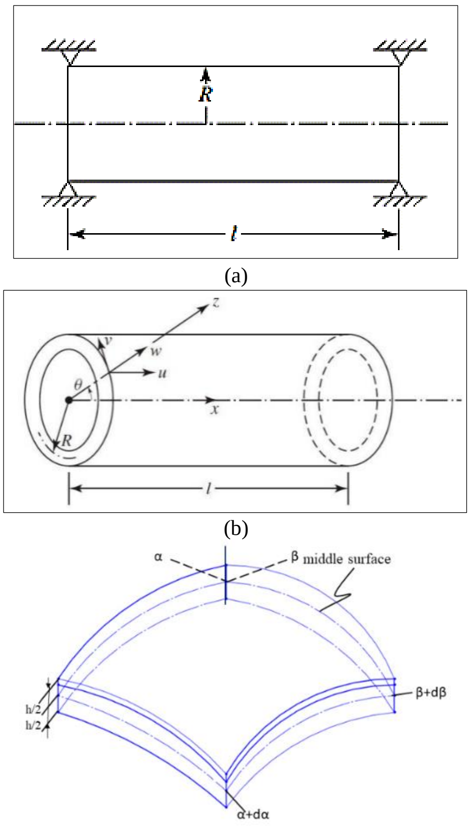

(a)

(b)

(c)

Fig. 5. The model's geometry used (a) Simply-supported BCs and (b-c) coordinates of a thin cylindrical shell

$$\bar{u}(\alpha,\beta,z,t) = u(\alpha,\beta,t) + z\theta_\alpha(\alpha,\beta,t)$$
$$\bar{v}(\alpha,\beta,z,t) = v(\alpha,\beta,t) + z\theta_\beta(\alpha,\beta,t) \qquad (2)$$
$$\bar{w}(\alpha,\beta,z,t) = w(\alpha,\beta,t)$$

The variables (u, v, and w) represent the shell's middle surface displacements along the directions α, β, and z, while R indicates the radius of the cylinder. The rotations of the intermediate surface normal about the α and β axes, denoted as θ_α and θ_β, can be determined as follows:

$$\theta_\alpha = \frac{\partial w}{\partial x} \qquad (3)$$
$$\theta_\beta = \frac{v}{R} - \frac{1}{R}\frac{\partial w}{\partial \theta}$$

For the cylindrical shell shown in Figure 5, with coordinates x, θ, and z, the parallel displacements along the cylindrical shell coordinate are denoted as u, v, and w, while the variables α and β represent x and θ, respectively, and h is the thickness of the shell. Thus, the general equation of motion for a cylindrical shell can be expressed as follows:

$$\left(\frac{\partial N_{xx}}{\partial x} + \frac{1}{R}\frac{\partial N_{\theta x}}{\partial \theta} + f_x\right) = \rho h\ddot{u}$$
$$\frac{\partial N_{x\theta}}{\partial x} + \frac{1}{R}\frac{\partial N_{\theta\theta}}{\partial \theta} + \frac{1}{R}\left(\frac{\partial M_{x\theta}}{\partial x} + \frac{1}{R}\frac{\partial M_{\theta\theta}}{\partial \theta}\right) + f_\theta = \rho h\ddot{v}$$
$$\frac{\partial^2 M_{xx}}{\partial x^2} + \frac{1}{R}\frac{\partial^2 M_{x\theta}}{\partial x\,\partial\theta} + \frac{1}{R^2}\frac{\partial^2 M_{\theta\theta}}{\partial \theta^2} - \frac{N_{\theta\theta}}{R} + f_z = \rho h\ddot{w} \qquad (4)$$

where, $N_{xx}, N_{\theta x}, N_{\theta\theta}, M_{xx}, M_{x\theta}$, and $M_{\theta\theta}$ are force and moment components, shown in Figure 6. The components are written as:

$$N_{xx} = C\left(\frac{\partial u}{\partial x} + \frac{\nu}{R}\frac{\partial v}{\partial \theta} + \frac{\nu}{R}w\right)$$
$$N_{\theta x} = C\frac{(1-\nu)}{2}\left(\frac{\partial v}{\partial x} + \frac{1}{R}\frac{\partial u}{\partial \theta}\right)$$
$$N_{\theta\theta} = C\left(\frac{1}{R}\frac{\partial v}{\partial \theta} + \frac{w}{R} + \nu\frac{\partial u}{\partial x}\right)$$
$$M_{xx} = D\left(-\frac{\partial^2 w}{\partial x^2} + \frac{\nu}{R^2}\frac{\partial v}{\partial \theta} - \frac{\nu}{R^2}\frac{\partial^2 w}{\partial \theta^2}\right) \qquad (5)$$
$$M_{x\theta} = D\left(\frac{(1-\nu)}{2}\right)\left(\frac{1}{R}\frac{\partial v}{\partial x} - \frac{2}{R}\frac{\partial^2 w}{\partial x\,\partial\theta}\right)$$
$$M_{\theta\theta} = D\left(\frac{1}{R^2}\frac{\partial v}{\partial \theta} - \frac{1}{R^2}\frac{\partial^2 w}{\partial \theta^2} - \nu\frac{\partial^2 w}{\partial x^2}\right)$$

where, $C = \frac{Eh}{(1-\nu^2)}$, and $D = \frac{Eh^3}{12(1-\nu^2)}$.

Shell materials have a modulus of elasticity (E) corresponding to their thickness and density, respectively; they also have a Poisson's ratio (ν) corresponding to the material, while external forces are (f_x, f_y, f_z).

Then, by inserting Equation (5) into Equation (4), for free vibration external forces $f_x, f_y, f_z = 0$, and by using Donnell-Mushtari Vlasov (DMV) theory, get

$$\frac{\partial^2 u}{\partial x^2} + \frac{(1-\nu)}{2R^2}\frac{\partial^2 u}{\partial \theta^2} + \frac{\nu}{R}\frac{\partial w}{\partial x} + \frac{(1+\nu)}{2R}\frac{\partial^2 v}{\partial x\,\partial\theta} = \frac{(1-\nu^2)}{E}\rho\frac{\partial^2 u}{\partial t^2}$$
$$\left\{\begin{array}{c} \frac{(1-\nu)}{2}\frac{\partial^2 v}{\partial x^2} + \frac{1}{R^2}\frac{\partial^2 v}{\partial \theta^2} + \frac{1}{R^2}\frac{\partial w}{\partial \theta} + \frac{(1+\nu)}{2R}\frac{\partial^2 u}{\partial x\,\partial\theta} = \frac{(1-\nu^2)}{E}\rho\frac{\partial^2 v}{\partial t^2} \\ -\left(\frac{\nu}{R}\frac{\partial u}{\partial x} + \frac{1}{R^2}\frac{\partial v}{\partial \theta} + \frac{w}{R^2}\right) - \frac{h^2}{12}\left(\frac{\partial^4 w}{\partial x^4} + \frac{2}{R^2}\frac{\partial^4 w}{\partial x^2\,\partial\theta^2} + \frac{1}{R^4}\frac{\partial^4 w}{\partial \theta^4}\right) \\ = \frac{(1-\nu^2)}{E}\rho\frac{\partial^2 w}{\partial t^2} \end{array}\right\} \qquad (6)$$

In Equation 6, (F) represents the bending load, (l) denotes the span length, (A) is the area of the beam's cross-section, and (G) represents the modulus of shear.

Therefore, with the aid of Equation 6 and the separation of variable technique, the shell displacement as a function of x and θ can be found. The following relations can be used for simply supported boundary conditions ($x = 0$ and $x = l$).

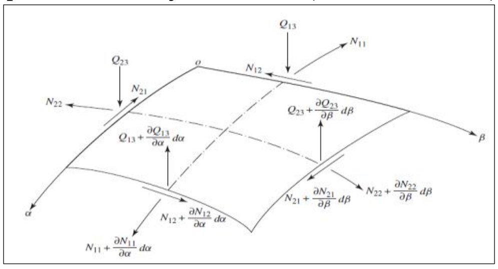

(a)

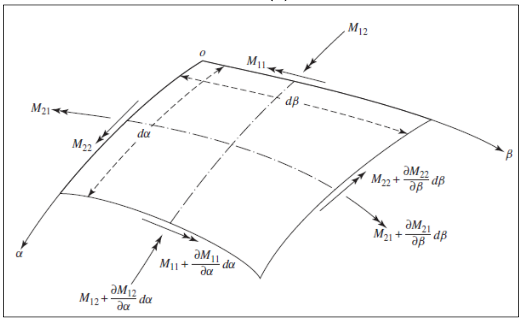

(b)

Fig. 6. (a) A shell force resultant (b) A resultant of the moment

$$v(0,\theta,t) = w(0,\theta,t) = 0$$
$$N_{xx}(0,\theta,t) = M_{xx}(0,\theta,t) = 0$$
$$v(l,\theta,t) = w(l,\theta,t) = 0 \qquad (7)$$
$$N_{xx}(l,\theta,t) = M_{xx}(l,\theta,t) = 0$$

Then, the components of displacement of the cylindrical shell can be represented by assuming the general form of harmonic function:

$$u(x,\theta,t) = \sum_m^\infty \sum_n^\infty A_{mn} \times Cos\frac{m\pi x}{l} \times Cos\, n\theta \times Cos\,\omega t$$
$$v(x,\theta,t) = \sum_m^\infty \sum_n^\infty B_{mn} \times Sin\frac{m\pi x}{l} \times Sin\, n\theta \times Cos\,\omega t$$
$$w(x,\theta,t) = \sum_m^\infty \sum_n^\infty C_{mn} \times Sin\frac{m\pi x}{l} \times Cos\, n\theta \times Cos\,\omega t \qquad (8)$$

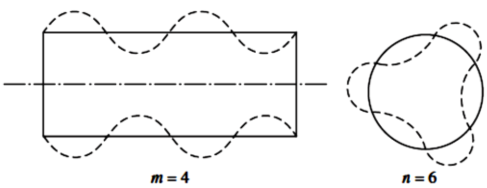

Fig.7. Displacement mode of a Shell

As depicted in Figure 7, m and n denote the wave characteristics of displacement along the length and circumference of the shell, respectively. By substituting Equation (8) into Equation (6), the following form was obtained:

$$\left(\begin{array}{c} -\left(\left(\frac{m\pi}{l}\right)^2 A_{mn}\, Cos\frac{m\pi x}{l} \times Cos\, n\theta\right) - \\ \left(\frac{(1-\nu)}{2R^2}(n)^2 A_{mn}\, Cos\frac{m\pi x}{l} \times Cos\, n\theta\right) + \\ \left(\frac{\nu}{R}\left(\frac{m\pi}{l}\right) C_{mn}\, Cos\frac{m\pi x}{l} \times Cos\, n\theta\right) \\ +\left(\frac{(1+\nu)}{2R}\left(\frac{m\pi}{l}\right)(n) B_{mn}\, Cos\frac{m\pi x}{l} \times Cos\, n\theta\right) \end{array}\right) Cos\,\omega t =$$
$$\left(-\frac{(1-\nu^2)}{E}\rho\omega^2 A_{mn}\, Cos\frac{m\pi x}{l} \times Cos\, n\theta\right) Cos\,\omega t$$

$$\left(\begin{array}{c} -\left(\frac{(1-\nu)}{2}\left(\frac{m\pi}{l}\right)^2 B_{mn}\times \mathrm{Sin}\frac{m\pi x}{l}\times \mathrm{Sin}\, n\theta\right) \\ -\left(\frac{1}{R^2}(n)^2 B_{mn}\times \mathrm{Sin}\frac{m\pi x}{l}\times \mathrm{Sin}\, n\theta\right)- \\ \left(\frac{1}{R^2}(n) C_{mn}\times \mathrm{Sin}\frac{m\pi x}{l}\times \mathrm{Sin}\, n\theta\right) \\ +\left(\frac{(1+\nu)}{2R}\left(\frac{m\pi}{l}\right)(n) A_{mn}\times \mathrm{Sin}\frac{m\pi x}{l}\times \mathrm{Sin}\, n\theta\right) \end{array}\right)\mathrm{Cos}\,\omega t = \left(-\frac{(1-\nu^2)}{E}\rho\omega^2 B_{mn}\times \mathrm{Sin}\frac{m\pi x}{l}\times \mathrm{Sin}\, n\theta\right)\mathrm{Cos}\,\omega t$$

$$\left(\begin{array}{c} \left(\frac{\nu}{R}\left(\frac{m\pi}{l}\right) A_{mn}\,\mathrm{Sin}\frac{m\pi x}{l}\times \mathrm{Cos}\, n\theta\right)- \\ \left(\frac{1}{R^2}(n) B_{mn}\,\mathrm{Sin}\frac{m\pi x}{l}\times \mathrm{Cos}\, n\theta\right)- \\ \left(\frac{1}{R^2} C_{mn}\,\mathrm{Sin}\frac{m\pi x}{l}\times \mathrm{Cos}\, n\theta\right)- \\ \left(\frac{h^2}{12}\left(\frac{m\pi}{l}\right)^4 C_{mn}\,\mathrm{Sin}\frac{m\pi x}{l}\times \mathrm{Cos}\, n\theta\right)- \\ \left(\frac{h^2}{12}\frac{2}{R^2}\left(\frac{m\pi}{l}\right)^2 (n)^2 C_{mn}\times \mathrm{Sin}\frac{m\pi x}{l}\times \mathrm{Cos}\, n\theta\right) \\ -\left(\frac{h^2}{12}\frac{1}{R^4}(n)^4 C_{mn}\times \mathrm{Sin}\frac{m\pi x}{l}\times \mathrm{Cos}\, n\theta\right) \end{array}\right)\mathrm{Cos}\,\omega t = \left(-\frac{(1-\nu^2)}{E}\rho\omega^2 C_{mn}\times \mathrm{Sin}\frac{m\pi x}{l}\times \mathrm{Cos}\, n\theta\right)\mathrm{Cos}\,\omega t \tag{9}$$

$$\begin{bmatrix} \left(\left(\frac{m\pi}{l}\right)^2+\frac{(1-\nu)}{2R^2}(n)^2 - \frac{(1-\nu^2)}{E}\rho\omega^2\right) & \left(-\frac{(1+\nu)}{2R}\left(\frac{m\pi}{l}\right)(n)\right) & \left(-\frac{\nu}{R}\left(\frac{m\pi}{l}\right)\right) \\ \left(-\frac{(1+\nu)}{2R}\left(\frac{m\pi}{l}\right)(n)\right) & \left(\frac{(1-\nu)}{2}\left(\frac{m\pi}{l}\right)^2+\frac{1}{R^2}(n)^2 - \frac{(1-\nu^2)}{E}\rho\omega^2\right) & \left(\frac{1}{R^2}(n)\right) \\ \left(-\frac{\nu}{R}\left(\frac{m\pi}{l}\right)\right) & \left(\frac{1}{R^2}(n)\right) & \left(\frac{1}{R^2}+\frac{h^2}{12}\left(\frac{m\pi}{l}\right)^4 + \frac{h^2}{12}\frac{2}{R^2}\left(\frac{m\pi}{l}\right)^2 (n)^2 + \frac{h^2}{12}\frac{1}{R^4}(n)^4 - \frac{(1-\nu^2)}{E}\rho\omega^2\right) \end{bmatrix} \begin{Bmatrix} A_{mn} \\ B_{mn} \\ C_{mn} \end{Bmatrix} = \begin{Bmatrix} 0 \\ 0 \\ 0 \end{Bmatrix} \tag{10}$$

$$\begin{vmatrix} \left(\left(\frac{m\pi}{l}\right)^2+\frac{(1-\nu)}{2R^2}(n)^2 - \frac{(1-\nu^2)}{E}\rho\omega^2\right) & \left(-\frac{(1+\nu)}{2R}\left(\frac{m\pi}{l}\right)(n)\right) & \left(-\frac{\nu}{R}\left(\frac{m\pi}{l}\right)\right) \\ \left(-\frac{(1+\nu)}{2R}\left(\frac{m\pi}{l}\right)(n)\right) & \left(\frac{(1-\nu)}{2}\left(\frac{m\pi}{l}\right)^2+\frac{1}{R^2}(n)^2 - \frac{(1-\nu^2)}{E}\rho\omega^2\right) & \left(\frac{1}{R^2}(n)\right) \\ \left(-\frac{\nu}{R}\left(\frac{m\pi}{l}\right)\right) & \left(\frac{1}{R^2}(n)\right) & \left(\frac{1}{R^2}+\frac{h^2}{12}\left(\frac{m\pi}{l}\right)^4 + \frac{h^2}{12}\frac{2}{R^2}\left(\frac{m\pi}{l}\right)^2 (n)^2 + \frac{h^2}{12}\frac{1}{R^4}(n)^4 - \frac{(1-\nu^2)}{E}\rho\omega^2\right) \end{vmatrix} = 0 \tag{11}$$

Or, Equation 11 may be arranged as,

$$\left(\begin{array}{c} \left(\left(\frac{m\pi}{l}\right)^2+\frac{(1-\nu)}{2R^2}(n)^2 - \frac{(1-\nu^2)}{E}\rho\omega^2\right)\left(\left(\frac{(1-\nu)}{2}\left(\frac{m\pi}{l}\right)^2 + \frac{1}{R^2}(n)^2 - \frac{(1-\nu^2)}{E}\rho\omega^2\right)\left(\frac{1}{R^2}+\frac{h^2}{12}\left(\frac{m\pi}{l}\right)^4 + \frac{h^2}{12}\frac{2}{R^2}\left(\frac{m\pi}{l}\right)^2 (n)^2 + \frac{h^2}{12}\frac{1}{R^4}(n)^4 - \frac{(1-\nu^2)}{E}\rho\omega^2\right) - \left(\frac{1}{R^2}(n)\right)^2\right) - \\ \left(-\frac{(1+\nu)}{2R}\left(\frac{m\pi}{l}\right)(n)\right)\left(\left(-\frac{(1+\nu)}{2R}\left(\frac{m\pi}{l}\right)(n)\right)\left(\frac{1}{R^2}+\frac{h^2}{12}\left(\frac{m\pi}{l}\right)^4 + \frac{h^2}{12}\frac{2}{R^2}\left(\frac{m\pi}{l}\right)^2 (n)^2 + \frac{h^2}{12}\frac{1}{R^4}(n)^4 - \frac{(1-\nu^2)}{E}\rho\omega^2\right) + \left(\frac{1}{R^2}(n)\right)\left(\frac{\nu}{R}\left(\frac{m\pi}{l}\right)\right)\right) - \\ \left(\frac{\nu}{R}\left(\frac{m\pi}{l}\right)\right)\left(\left(-\frac{(1+\nu)}{2R}\left(\frac{m\pi}{l}\right)(n)\right)\left(\frac{1}{R^2}(n)\right) + \left(\frac{(1-\nu)}{2}\left(\frac{m\pi}{l}\right)^2 + \frac{1}{R^2}(n)^2 - \frac{(1-\nu^2)}{E}\rho\omega^2\right)\left(\frac{\nu}{R}\left(\frac{m\pi}{l}\right)\right)\right) \end{array}\right) = 0 \tag{12}$$

Then, by solution, Equation 12 may be used to estimate the natural frequency for a model $\alpha, \beta,$ and z-direction, with various modulus of elasticity value and different nanoparticle materials effect.

4. NUMERICAL SIMULATION

With Finite Element Methods (FEMs), numerical findings can be compared with those gained through experiments. The ANSYS software 2021 R1 was used to perform a modal analysis of a composite cylindrical structure. Using the Solid186 shell model, 1692 shell elements were generated, and meshing was performed, as shown in Figure 8; shell end conditions were selected, and modal analyses were conducted for each desired model [42-45]. The experimental work yields the mechanical properties used in the engineering data view. Analytical techniques (Equation 12) and numerical approaches (FEM) can be used to calculate the natural frequency of shell structures. Table 1 shows two groups composed of different layers of composite materials reinforced with nanoparticles.

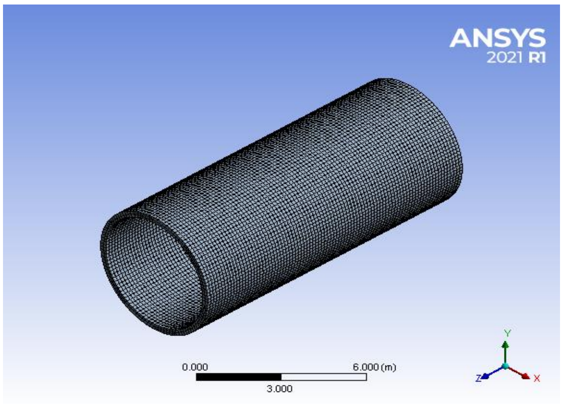

Fig. 8. A 3D model with a mesh

5. RESULTS AND DISCUSSION

The main objective of this investigation is to modify the mechanical vibration characteristics of composite shell structures with a high volume fraction of the nanoparticle materials. To enhance the mechanical performance of such structures to be used in engineering applications. The influence of reinforced nanoparticles in the composite shell (Nano Al_2O_3 and Nano SiO_2) is determined using analytical and numerical approaches.

Adding two layers of Kenaf to group B at the expense of Perlon layers in group A led to an increase in Young's modulus, meaning good material strength of composite samples from (16.78 to 17.49) GPa with a percentage increase of 4.23%. The addition of the volume fraction of nano Al_2O_3 and nano SiO_2 in groups A and B of the composite shell at value (0-2.5)% gave a direct relationship. The higher the volume fraction, the better the resistance of the composite material, the improved the modulus of elasticity (22.47 and 24.13) GPa of Al_2O_3 and (23.87 and 25.78) GPa of SiO_2 at 2.5% volume fraction.

Table 4 shows that adding SiO_2 nanoparticles had the highest modulus of elasticity (23.87 and 25.78) GPa of SiO_2 compared to (22.47 and 24.13) GPa of Al_2O_3 nanoparticles. As a result, as shown in Table 4, the inclusion of SiO_2 nanoparticles in group B enhances the modulus of elasticity by 47.39 percent at a volume fraction of 2.5 percent.

Table 4. Variation in modulus of elasticity with and without reinforcements

Group	E (GPa) Without Nano	E (GPa) Al_2O_3 Nano	Incr. %	E (GPa) SiO_2 Nano	Incr. %
A	16.78	22.47	33.90	23.87	42.25
B	17.49	24.13	37.96	25.78	47.39

Figure 9 demonstrates the effect of adding nanoparticles SiO_2 and Al_2O_3 to the composite shell on the elastic modulus. Based on the findings, groups A and B show good agreement between the numerical and analytical natural frequencies. Furthermore, it has been observed that the presence of SiO_2 nanoparticles increases the natural frequency to a greater extent than the effect of Al_2O_3 nanoparticles in both groups. The possible reason is due to the nature of the microstructure of Si and Al. However, group B recorded the highest natural frequency of 5780 rad/sec for SiO_2 nano particles at a volume fraction of 2.5%. Figure 10 shows the effect of nanoparticle reinforcements on composite shell structures by comparing analytical and numerical frequency results.

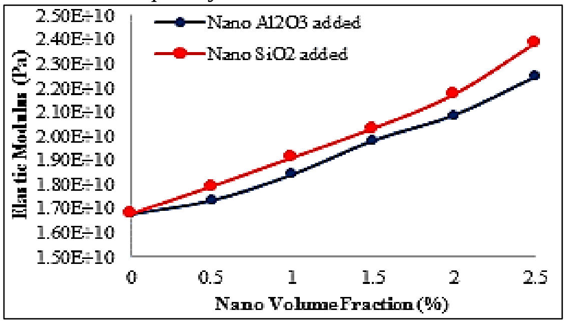

a. Group A

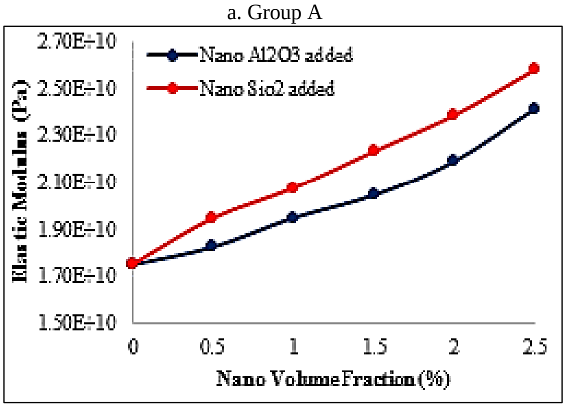

b. Group B

Fig. 9. Various composite shell groups exhibit different elastic modulus variations with nano volume fractions

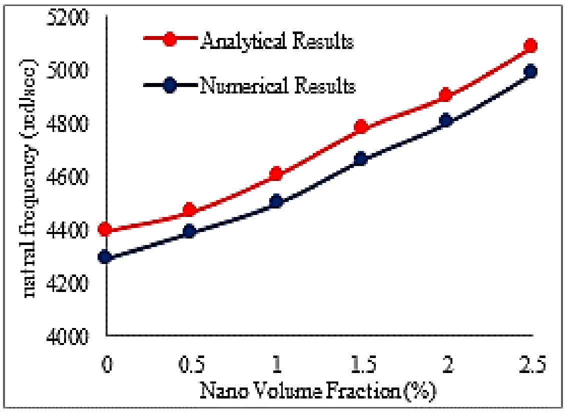

a. Group A, (Al2O3) nanomaterial

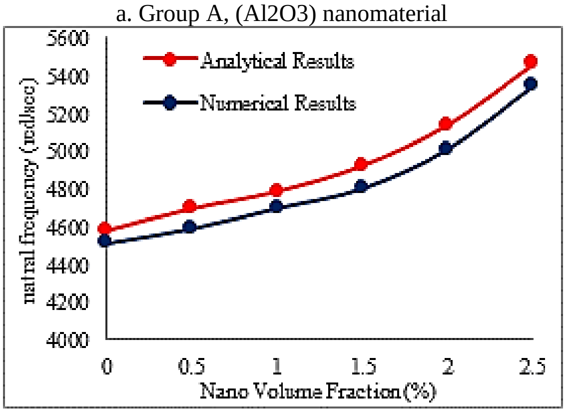

b. Group B, (Al2O3) nanomaterial

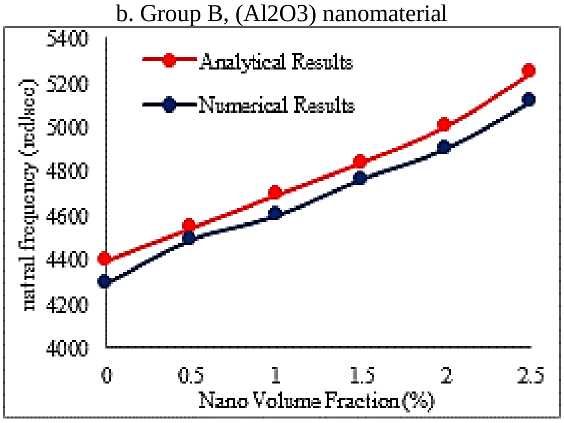

c. Group A, (SiO2) nanoparticles

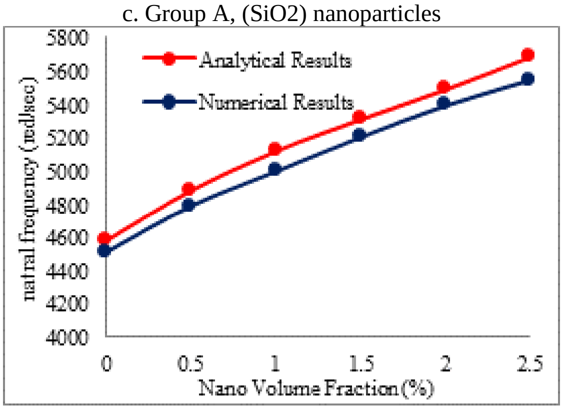

d. Group B, (SiO_2) nanoparticles

Fig. 10. The impacts of nanoparticle materials on composite shell structures by comparing analytical and numerical frequency results

Figure 11 shows the numerical and analytical results of the natural frequency for two groups (A and B) based on the concentration of both nanoparticles, SiO_2 and Al_2O_3. The results show a clear improvement in the natural frequency of shells with SiO_2 nanoparticles rather than Al_2O_3.

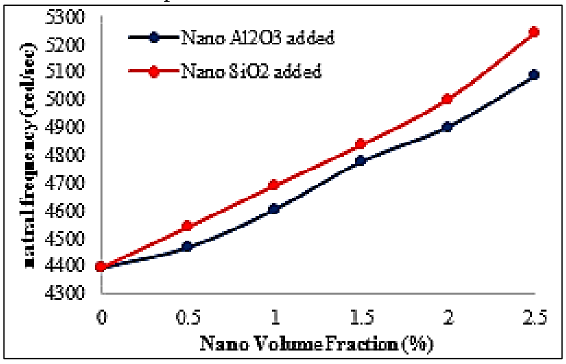

a. Group A

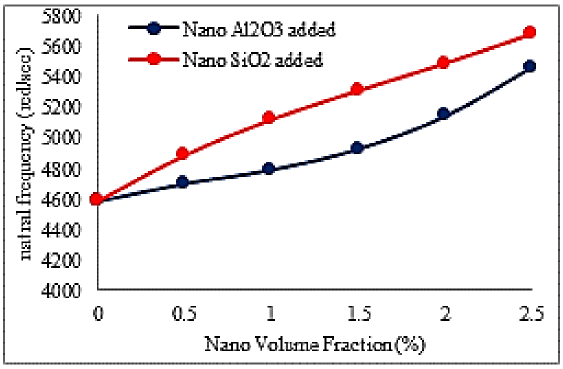

b. Group B

Fig. 11. Free variation analysis of the composite shell types A and B with different nano volume fractions

Normalized natural frequency results have been obtained when studying the free vibration of a cylindrical shell with varied BCs [30]:

$$\psi = \omega.R\sqrt{\rho(1-\nu^2)/E} \tag{13}$$

Figure 12 illustrates the numerical outcomes of the frequency parameter for the composite shell group (A) at a ratio of (L/R = 5) with five different boundary conditions (BCs). Based on the obtained results, it is evident that the frequency coefficient value rises as the number of restrictions in the chosen model increases. This finding indicates an increase in the overall strength of the shell model.

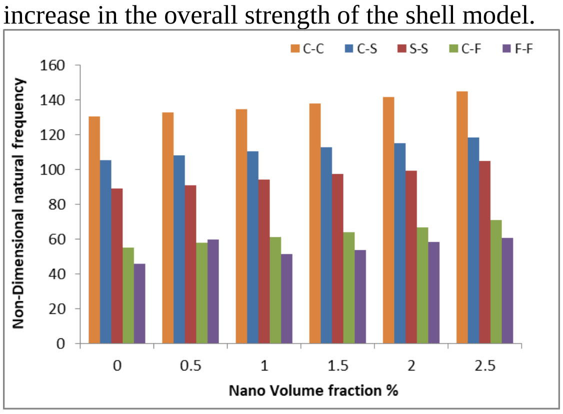

Fig. 12. Results for the frequency parameter (Group A) subjected to various BCs

SEM has been widely used to examine surface topology and nanoparticles. Different materials containing nanoparticles of known distribution were analyzed to test the accuracy of an analytical model using high-resolution SEM. Figure 13 shows SEM images of Group A with Nano SiO_2 with different magnifications (1 µm and 2 µm). Figures 14-16 show SEM images of Group A with nano Al_2O_3 and SiO_2 material with different magnifications, respectively. From the results, one can see the distribution of fibers into the matrix phase. Different magnifications of SEM images are presented that illustrate the reinforcement distribution and binding of phases.

Moreover, it can be seen that SiO_2 images exhibit stronger borders and more contrast than Al_2O_3. Also, it is observed that a good transmission contrast is observed between the two types of nanoparticles. High-resolution SEM imaging can define nanoparticles' morphology, characteristics, and interior structure.

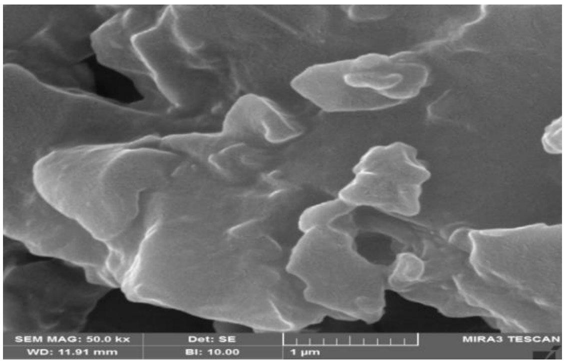

a. 1 µm

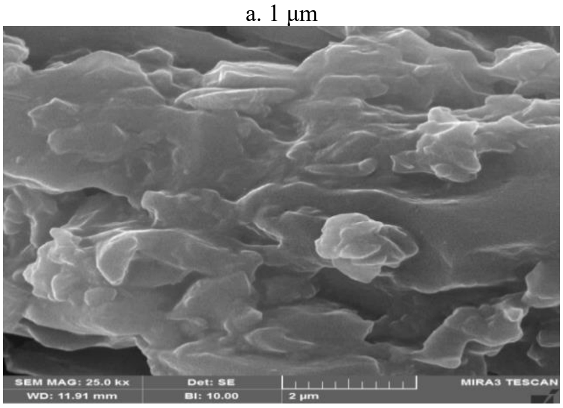

b. 2µm

Fig. 13. SEM images of Group A with Nano SiO_2 with different magnifications

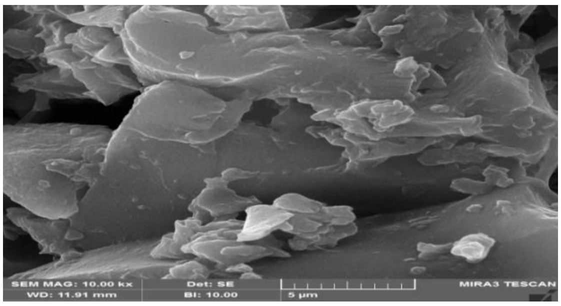

a. 5 µm

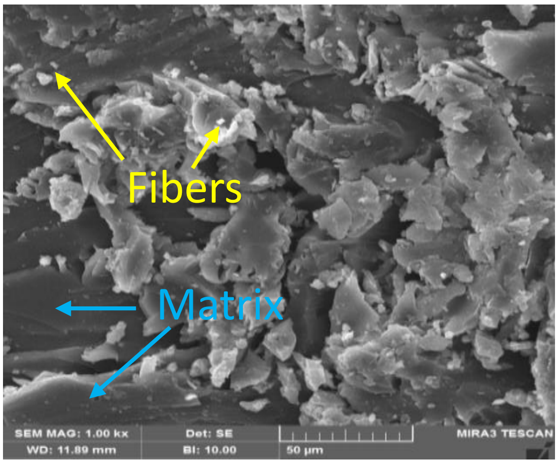

b. 50 µm
Fig. 14. SEM images of Group A with nano Al_2O_3 Material with different magnification

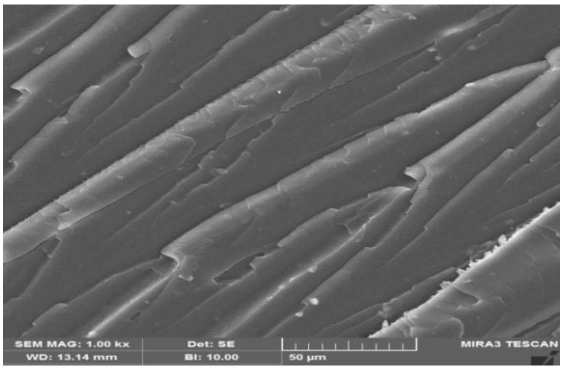

a. 50 µm

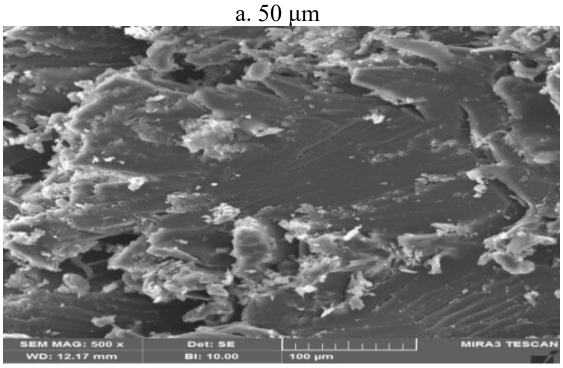

b. 100 µm
Fig. 15. Different magnifications of SEM images of Group B with nano Al2O3 Material

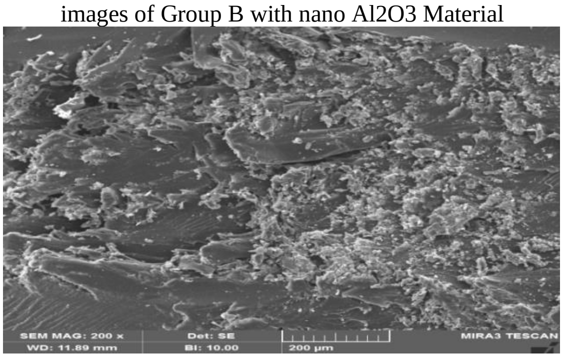

b. 200 µm

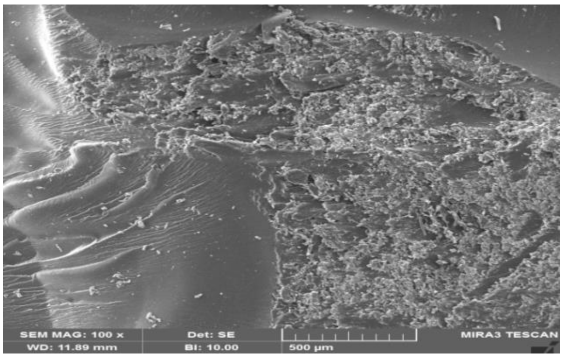

b. 500 µm
Fig. 16. Different magnifications of SEM images of Group B with nano SiO_2 Material

4. CONCLUSION

The addition of nano Al_2O_3 and Nano SiO_2 reinforced composite cylindrical shells for groups A and B is covered in detail in this work. There are several interpretations can be recorded to sustain the nanocomposite shell, mechanical and natural frequency properties, including:

1. The modulus elasticity values of the composite shell material in groups A and B were increased by adding small nano-volume fractions of nanoscale Al_2O_3 and nanoscale SiO_2 nanoparticles.
2. The molecular bonds between the shell composite material particles are strengthened by the nanoparticles that permeate between them, contributing to the increased strength of the two groups' composite shell material.
3. The addition of nano Al_2O_3 and nano SiO_2 nanoparticles increases the natural frequency of the shell due to the sitting of nanoparticles through voids of composite materials. This increases the bonding strength between particles and grains in the atomic structure of the composite material's shell. Two composite materials were strengthened by the addition of nanoparticle materials, resulting in a roughly 30% increase in natural frequency.
4. Adding nano volume fraction to the composite materials in a shell increases the modulus of elasticity values which in turn increases the natural frequency of a composite.
5. By comparing the results, adding nano SiO_2 increases the modulus of elasticity, and vibration characteristics that increase the shell's strength better than nano Al_2O_3.
6. Free vibration analysis by employing the analytical and numerical techniques shows good agreement between each other with a maximum difference of 5%.

Source of funding: *This research received no external funding.*

Author contributions: *Research concept and design, E.K.; Collection and/or assembly of data, Z.A.;*

Writing the article, M.A.; Critical revision of the article, R.M.; Final approval of the article, E.N.

Declaration of competing interest: *The authors declare that they have no known competing financial interests or personal relationships that could have appeared to influence the work reported in this paper.*

REFERENCES

1. Njim EK, Bakhy SH, Al-Waily M. Experimental and numerical flexural analysis of porous functionally graded beams reinforced by (Al/Al_2O_3) nanoparticles. International Journal of Nanoelectronics and Materials. 2022;15:91-106.
2. Jawad K. Oleiwi, Nesreen Dakhel Fahad, Marwah Mohammed Abdulridha, Muhannad Al-Waily, Emad Kadum Njim, Laser Treatment Effect on Fatigue Characterizations for Steel Alloy Beam Coated with Nanoparticles, International Journal of Nanoelectronics and Materials. 2023;16:105-119.
3. Al-Shablle M, Al-Waily M, Njim EK, Analytical evaluation of the influence of adding rubber layers on free vibration of sandwich structure with the presence of nano-reinforced composite skins," Archives of Materials Science and Engineering. 2023;116(2): 57-70. https://doi.org/10.5604/01.3001.0016.1190.
4. Zhang H, Li M, Hu W, An X, Fan H. Nondestructive parameter identification technique of ultra-light CFRC corrugated sandwich cylinder, NDT & E International. 2021;124:102520. https://doi.org/10.1016/j.ndteint.2021.102520.
5. Zhang D et al. Lower-bound axial buckling load prediction for isotropic cylindrical shells using probabilistic random perturbation load approach. Thin-Walled Structures. 2020;155:106925. https://doi.org/10.1016/j.tws.2020.106925.
6. Licai Yang, Ying Luo, Tian Qiu, Hao Zheng, Peng Zeng, A novel analytical study on the buckling of cylindrical shells subjected to arbitrarily distributed external pressure. Eur. J. Mech. Solid. 2022. https://doi.org/10.1016/j.euromechsol.2021.104406.
7. Li M, Fan H. Free vibration behaviors and vibration correlation technique of hierarchical Isogrid stiffened composite cylinders. Thin-Walled Structures. 2021; 159: 107321. https://doi.org/10.1016/j.tws.2020.107321.
8. Al-Waily M, Al-Shammari, MA, Jweeg MJ, An analytical investigation of thermal buckling behavior of composite plates reinforced by carbon nano particles. Engineering Journal. 2020;24(3):11–21. https://doi.org/10.4186/ej.2020.24.3.11.
9. Raad H, Njim E, Jweeg M, Al-Waily M, Hadji L, Madan R. Vibration analysis of sandwich plates with hybrid composite cores combining porous polymer and foam structures. JCAM 2024;55(3). https://doi.org/10.22059/jcamech.2024.377658.1121.
10. Al-Shablle M, Njim EK, Jweeg MJ, Al-Waily M. Free vibration analysis of composite face sandwich plate strengthens by Al_2O_3 and SiO_2 nanoparticles materials. Diagnostyka. 2023;24(2):1–9. https://doi.org/10.29354/diag/162580.
11. Javed S, Viswanathan KK, Aziz ZA. Free vibration analysis of composite cylindrical shells with non-uniform thickness walls. Steel and Composite Structures. 2016;20(5):1087-1102. https://doi.org/10.12989/scs.2016.20.5.1087.
12. Helloty AE. Dynamic response of laminated composite shells subjected to impulsive loads. IOSR Journal of Mechanical and Civil Engineering. 2017;14 (3):108-113. https://doi.org/10.9790/1684-140301108123.
13. Chaubey AK, Kumar A, Chakrabarti A. Vibration of laminated composite shells with cutouts and concentrated mass. AIAA Journal. 2018;56(4):1662–1678. https://doi.org/10.2514/1.J056320.
14. Haichao Li, Fuzhen Pang, Hailong Chen, Yuan D. Vibration analysis of functionally graded porous cylindrical shell with arbitrary boundary restraints by using a semi analytical method, Composites Part B: Engineering. 2019;164:249–264. https://doi.org/10.1016/j.compositesb.2018.11.046.
15. Wang YQ, Ye C, Zu JW. Vibration analysis of circular cylindrical shells made of metal foams under various boundary conditions, International Journal of Mechanics and Materials in Design. 2019;15(2):333–344. https://doi.org/10.1007/s10999-018-9415-8.
16. Dongze He, Dongyan Shi, Qingshan Wang, Cijun Shuai. Wave based method (WBM) for free vibration analysis of cross-ply composite laminated cylindrical shells with arbitrary boundaries. Composite Structures. 2019;213:284–298. https://doi.org/10.1016/j.compstruct.2019.01.088.
17. Ghasemi AR, Mohandes M. Free vibration analysis of micro and nano fiber-metal laminates circular cylindrical shells based on modified couple stress theory, Mechanics of Advanced Materials and Structures. 2018;27(1):43–54. https://doi.org/10.1080/15376494.2018.1472337.
18. Trung Thanh Tran, Van Ke Tran, Pham Binh Le, Van Minh Phung, Van Thom Do and Hoang Nam Nguyen, Forced Vibration Analysis of Laminated Composite Shells Reinforced with Graphene Nanoplatelets Using Finite Element Method. Advances in Civil Engineering 2020;1–17. http://dx.doi.org/10.1155/2020/1471037.
19. Zhang C, et al. Vibration analysis of a sandwich cylindrical shell in hygrothermal environment, Nanotechnology Reviews. 2021;10(1):414–430. https://doi.org/10.1515/ntrev-2021-0026.
20. Shibai Guo, Ping Hu, Sheng Li. The walsh series discretization method for free vibration analysis of composite spherical shells based on the shear deformation theory. Composite Structures. 2022;288: 115408. https://doi.org/10.1016/j.compstruct.2022.115408.
21. Wu MQ, Zhang W, Niu Y. Experimental and numerical studies on nonlinear vibrations and dynamic snap-through phenomena of bistable asymmetric composite laminated shallow shell under center foundation excitation. European Journal of Mechanics - A/Solids. 2021;89. https://doi.org/10.1016/j.euromechsol.2021.104303.
22. Chen W, Luo WM, Chen SY, Peng LX, A FSDT meshfree method for free vibration analysis of arbitrary laminated composite shells and spatial structures. Composite Structures. 2022;279. https://doi.org/10.1016/j.compstruct.2021.114763.
23. Mohammadi H, Setoodeh AR, Vassilopoulos AP. Isogeometric Kirchhoff–Love shell patches in free and forced vibration of sinusoidally corrugated FG carbon nanotube-reinforced composite panels. Thin-Walled Structures. 2022;171:108707. https://doi.org/10.1016/j.tws.2021.108707.

24. Melaibari A. et al. A dynamic analysis of randomly oriented functionally graded carbon nanotubes/fiber-reinforced composite laminated shells with different geometries. Mathematics. 2022;10(3):408. https://doi.org/10.3390/math10030408.
25. Tian K, Huang L, Sun Y, Zhao L, Gao T, Wang B. Combined approximation based numerical vibration correlation technique for axially loaded cylindrical shells. European Journal of Mechanics - A/Solids. 2022;93:104553. https://doi.org/10.1016/j.euromechsol.2022.104553.
26. Lin G, et al. Dynamic instability of fiber composite cylindrical shell with metal liner subjected to internal pulse loading. Composite Structures. 2022;280: 114906. https://doi.org/10.1016/j.compstruct.2021.114906.
27. Li H, Pang F, Miao X, Gao S, Liu F. A semi analytical method for free vibration analysis of composite laminated cylindrical and spherical shells with complex boundary conditions. Thin-Walled Structures. 2019;136:200–220. https://doi.org/10.1016/j.tws.2018.12.009.
28. Sandipan Nath Thakur, Chaitali Ray, Static and free vibration analyses of moderately thick hyperbolic paraboloidal cross ply laminated composite shell structure. Structures 2021;32:876–888. https://doi.org/10.1016/j.istruc.2021.03.066.
29. Zamani HA. Free vibration of rotating graphene-reinforced laminated composite conical shells. Composites Part C: Open Access 2021;5:100153. https://doi.org/10.1016/j.jcomc.2021.100153.
30. Kim K, Jon Y, An K, Kwak S, Han Y. A solution method for free vibration analysis of coupled laminated composite elliptical-cylindrical-elliptical shell with elastic boundary conditions. Journal of Ocean Engineering and Science 2022;7(2):112–130. https://doi.org/10.1016/j.joes.2021.07.005.
31. Guo C, Liu T, Wang Q, Qin B, Wang A. A unified strong spectral Tchebychev solution for predicting the free vibration characteristics of cylindrical shells with stepped-thickness and internal-external stiffeners. Thin-Walled Structures. 2021;68:108307. https://doi.org/10.1016/j.tws.2021.108307.
32. Logesh K, Vel VM, Seikh AH, Hebbale AM, Nagabhooshanam SANA, Subbiah R, Siddique MH, Praveen Kumar S. Investigations of nanoparticles (Al_2O_3-SiO_2) addition on the mechanical properties of blended matrix polymer composite. Journal of Nanomaterials. 2022(1):4392371. https://doi.org/10.1155/2022/4392371.
33. Sobhani E, Masoodi AR. A Comprehensive shell approach for vibration of porous nano-enriched polymer composite coupled spheroidal-cylindrical shells. Composite Structures. 2022;289:115464. https://doi.org/10.1016/j.compstruct.2022.115464.
34. Aurélien C, Juvé V, Mongin D, Maioli P, Fatti ND, Vallée F. Vibrations of spherical core-shell nanoparticles. Phys. Rev. 2011;B83(20):205430. https://doi.org/10.1103/PhysRevB.83.205430.
35. Jweeg Muhsin J, Njim EK, Abdullah OS, Al-Shammari MA, Al-Waily M, Bakhy SH. Free vibration analysis of composite cylindrical shell reinforced with silicon nano-particles: Analytical and FEM approach. Physics and Chemistry of Solid State. 2023;24(1):26–33. https://doi.org/10.15330/pcss.24.1.26-33.
36. Bhattacharyya M, Kapuria S, Kumar AN. On the stress to strain transfer ratio and elastic deflection behavior for Al/SiC functionally graded material. Mechanics of Advanced Materials and Structures. 2007;14(4):295–302. https://doi.org/10.1080/15376490600817917.
37. Madan Royal, Shubhankar Bhowmick. Modeling of functionally graded materials to estimate effective thermo-mechanical properties. World Journal of Engineering ahead-of-print (ahead-of-print). 2021. https://doi.org/10.1108/WJE-09-2020-0445.
38. Pershin V. et al, Simulation of graphene-containing viscous fluid motion in the gap between static and rotating discs. Journal of Physics: Conference Series 2019;1278(1):012025. https://doi.org/10.1088/1742-6596/1278/1/012025.
39. Pershin VF, et al. Production of few-layer and multilayer graphene by shearing exfoliation of graphite in liquids. IOP Conference Series: Materials Science and Engineering. 2019;693(1):012023. https://doi.org/10.1088/1757-899X/693/1/012023.
40. Shakouri M. Free vibration analysis of functionally graded rotating conical shells in thermal environment. Compos Part B-Eng. 2019;163:574-584. https://doi.org/10.1016/j.compositesb.2019.01.007.
41. Singiresu S. Rao. Vibration of continuous systems. John Wiley & Sons, Inc. 2007. https://doi.org/10.1002/9780470117866.
42. Raad H, Al-Waily M, Njim EK. Free vibration analysis of sandwich plate-reinforced foam core adopting micro aluminum powder. Physics and Chemistry of Solid State. 2022;23(4):659–668. https://doi.org/10.15330/pcss.23.4.659-668.
43. Jebur QH, Hamzah MN, Jweeg MJ, Njim EK, Al-Waily M, Resan KK. Modeling hyperplastic elastomer materials used in tire compounds: Numerical and experimental study. Jurnal Teknologi. 2024;86(5). https://doi.org/10.11113/jurnalteknologi.v86.21003.
44. Rahmani A, Faroughi S, Friswell MI. The vibration of two-dimensional imperfect functionally graded (2D-FG) porous rotating nanobeams based on general nonlocal theory. Mechanical Systems, and Signal Processing. 2020;144. https://doi.org/10.1016/j.ymssp.2020.106854.
45. Neamah RA, Al-Raheem SK, Njim EK, Abboud Z, Al-Ansari LS. Experimental and numerical investigation of the natural frequency for the intact and cracked laminated composite beam. Journal of Aerospace Technology and Management. 2024;16. https://doi.org/10.1590/jatm.v16.1337.

Ehab N. ABBAS
Assistant Prof. in Mechanical Engineering, Ministry of Higher Education and Scientific Research, Studies & Planning & Follow-Up Directorate, Baghdad, Iraq.
e-mail:
ehab_studies@mohesr.gov.iq

Zaman Abud Almalik ABUD ALI Doctor in Mechanical Engineering, Faculty of Engineering (Department of Mechanical Engineering) at the Kufa University, Iraq.
e-mail:
zaman.alhilo@uokufa.edu.iq

Emad Kadum NJIM. Senior Researcher in Mechanical Engineering-Applied Mechanics at the Ministry of Industry and Minerals, State Company for Tire Industry, Development and Research Department, Iraq.
e-mail:
emad- njim@scrit.gov.iq

Mujtaba A. FLAYYIH
Doctor in Mechanical Engineering, Prosthetics and Orthotics Engineering Department, College of Engineering and Technologies, Al-Mustaqbal University, Hillah, 51001, Iraq.

e-mail: mujtaba_abdulkadhim@uomus.edu.iq

Royal MADAN
Assistant Professor in the Mechanical Engineering Department at Graphic Era (Deemed to be University), located in Dehradun, India.
e-mail:
royalmadan.me@geu.ac.in